



# Geophysical Research Letters®



## RESEARCH LETTER

10.1029/2023GL105224

## Space-Time Inconsistencies in the Dynamics of Water Coverage: Tracking Walking Floods

Paula Torre Zaffaroni<sup>1,2,3</sup> , Javier Houspanossian<sup>3</sup>, Carlos M. Di Bella<sup>1,2</sup> , and Esteban G. Jobbágy<sup>3</sup>

<sup>1</sup>Instituto de Investigaciones Fisiológicas y Ecológicas Vinculadas a la Agricultura (IFEVA), Facultad de Agronomía, Universidad de Buenos Aires, CONICET, Buenos Aires, Argentina, <sup>2</sup>Departamento de Métodos Cuantitativos y Sistemas de Información, Facultad de Agronomía, Universidad de Buenos Aires, Buenos Aires, Argentina, <sup>3</sup>Grupo de Estudios Ambientales—IMASL, Universidad Nacional de San Luis, CONICET, San Luis, Argentina

### Key Points:

- We developed two complementary indices to describe water cover shifts between and within flooding events
- Over the last 36 years, shifts expanded the global flooded-affected area by 25% with another 20% redistributing at intermediate stages
- Flat topographies, arid climates, and irrigation favor this phenomenon while river dams and channels inhibit it over time

### Supporting Information:

Supporting Information may be found in the online version of this article.

### Correspondence to:

P. Torre Zaffaroni,  
[torrezaffaroni@agro.uba.ar](mailto:torrezaffaroni@agro.uba.ar)

### Citation:

Torre Zaffaroni, P., Houspanossian, J., Di Bella, C. M., & Jobbágy, E. G. (2023). Space-time inconsistencies in the dynamics of water coverage: Tracking walking floods. *Geophysical Research Letters*, 50, e2023GL105224. <https://doi.org/10.1029/2023GL105224>

Received 28 JUN 2023  
Accepted 28 NOV 2023

**Abstract** Floods in ideal landscapes follow a coherent pattern where single water-covered areas expand and afterward recede following the inverse sequence, but deviate in real landscapes due to natural or human factors resulting in water coverage shifts. Using remote sensing, we introduced two indices to describe the discrepancies between spatially integrated versus pixel-level frequency distributions under maximum inundated conditions ( $d_{ext}$ ) and throughout all flooding conditions ( $d_{tot}$ ), expressed as the relative weight of shifts on each landscape's maximum registered coverage, theoretically ranging between no displacement (<20%) to maximum displacement ( $\ll \infty$ ). Globally, over 36 years inundations exhibited redistributions representing, on average, 25% and 45% of their peak extents revealing previously unnoticed extra engaged areas and rotational movements within events, rising up to 500% in meandering rivers (South America) and irrigated croplands (Central Asia). We also assessed the influence of natural and human variables and discussed the indices' potential for advancing flood research.

**Plain Language Summary** While in ideal landscapes surface water should display the same spatial distribution across the expansion and recession stages of any flooding event, real dynamics may drift away from this expected pattern. We developed two indices based on remote sensing data to locate where these shifts are important and understand how they are influenced by nature and humans. By analyzing data from around the world, we discovered that thanks to the displacement from the ideal distributions, surface water covered globally an extra quarter of the area. Natural factors like low terrain ruggedness and high aridity foster much larger inundation displacement. In regions hosting rivers that carry large quantities of sediment and often change their course (e.g., India and Perú), displacement engages five times more area in floods than expected. We also found that water infrastructure like reservoirs and irrigation also influenced inundation displacement. For instance, displacement was very relevant in intensely irrigated regions like Central Asia and Australia, reflecting surface water deviation as needed for crop production. Because these variations scope water's spatiotemporal dynamics with important implications for the provision of many ecosystem services, their quantification and assessment allow us to monitor and understand our ongoing imprint on regional inundation dynamics.

## 1. Introduction

The spatial dynamics of floods, and specifically the pattern of their expansion and recession over the territory, is an important aspect of flooding variability. The flood pulse concept describes a model of flooding where water increasingly covers adjacent areas of already flooded surfaces, and afterward recedes following the exact inverse sequence, along what is described as an aquatic-terrestrial transition zone (Junk et al., 1989; Wantzen et al., 2008, for a definition extended to lentic systems). This null model of fully coherent expansion/recession implies that the exact locations that are covered by water can be known for any level of flooding (i.e., any given fraction of water coverage) based on the distribution of previous events. However, in real landscapes like those occupied by alluvial fans with highly meandering rivers, water does not always proceed in this predictable way, changing locations throughout successive events or by following asymmetrical expansion versus recession trajectories (Finotello et al., 2020; Tockner et al., 2000). Though it could give important insights into ecosystem functioning at multiple levels, this attribute of surface water dynamics (hereafter, inundation displacement) has not yet been systematically quantified and has been seldom described in the case of shallow lakes. Instead, inundation displacement has been analyzed in riverbanks through numerical modeling (Camporeale et al., 2005), manual and automatized

© 2023 The Authors.

This is an open access article under the terms of the [Creative Commons Attribution-NonCommercial License](https://creativecommons.org/licenses/by-nc/4.0/), which permits use, distribution and reproduction in any medium, provided the original work is properly cited and is not used for commercial purposes.

detection of spatial shifts of water-classified pixels (Langhorst & Pavelsky, 2023; Lin et al., 2020), or, more commonly, included as a known attribute in the design of field experiments and observations (Constantine & Dunne, 2008; Finotello et al., 2020; Walcker et al., 2021) from which a large body of knowledge on the physical laws guiding displacement has been generated (Van Dijk et al., 2013; Wren et al., 2008).

The spatiotemporal nature of this phenomenon suggests that it can be explored through remote sensing. A key advantage is its ability to uniformly study one attribute with low costs. With the development of global water masks from the Landsat satellite archive (Pekel et al., 2016a) and cloud processing servers (Gorelick et al., 2017), it is possible to analyze displacement globally for more than three decades. Such information has already helped to explore surface water's temporal dynamics, including long-term trends (Olthof & Rainville, 2022; Pekel et al., 2016a), other components of temporal variability (Pickens et al., 2020; Torre Zaffaroni, Baldi, et al., 2023), and even colorimetric characterizations as a proxy of water quality (Gardner et al., 2021). Moreover, Langhorst and Pavelsky (2023) have shown that the displacement of riverbeds can be assessed through remote sensing, quantifying the direction of erosion and accretion for water courses wider than 100 m with excellent results. These studies showcase how optical remote sensing tools can detect detailed aspects of surface water, presenting an opportunity for comprehensive global characterizations and studies of geographical drivers, despite their limitations such as data gaps caused by cloud coverage and lower resolution for older satellite missions.

While climate, topography, and water infrastructure have been pointed out as drivers of inundation displacement, their relative importance in dictating how patterns drift away from a coherent regime remains unquantified. In the case of dry regions, high runoff and precipitation variability translate into spatially heterogeneous flood events (Brunsell, 2010; Tooth, 2000). Rivers in plains with high geomorphological activity can carry, remove, and deposit large amounts of sediment in their banks fostering migration of courses and the formation of oxbow lakes which retain large masses of water (Constantine & Dunne, 2008; Langhorst & Pavelsky, 2023; Richardson et al., 1987). Because slope, ruggedness, and landforms at a landscape level dictate surface water transport and storage (McGuire et al., 2005; Rudorff et al., 2014; Sivapalan et al., 2011), we hypothesize that topographic characteristics are important determinants of inundation displacement beyond lotic systems. On top of natural drivers, irrigation, particularly in paddy rice cultivation, can contribute to inundation displacement due to varying watering practices in different plots, especially in regions that practice double and triple cropping systems (Dong et al., 2015; Sakamoto et al., 2007). River engineering, such as channelization, canalization, dams, and reservoirs can minimize inundation displacement by altering river geomorphology and sediment transport downstream (Tena et al., 2020; Vörösmarty et al., 2010; Ward & Stanford, 1995).

As surface water's expansion/recession cycles sustain many ecosystemic functions (Pi et al., 2022; Tockner & Stanford, 2002) including the exchange of greenhouse gases with the atmosphere (Saunois et al., 2020; Walcker et al., 2021; Watts et al., 2014), it is important to quantify how it displaces over time to better forecast changes in ecosystem function as well as global climate. Remote sensing tools make it feasible to monitor the response of inundations to increasingly variable precipitation regimes (Arias et al., 2021; Kundzewicz, 2008; Najibi & Devineni, 2018), changes in land use and land cover (Kuppel et al., 2015; Loarie et al., 2011; Twine et al., 2004), and mitigation-oriented water management strategies. It can further improve decision-making for water management and planning by improving the identification of flood-prone areas and their shift across landscapes.

This work addresses the spatial dynamics of surface water coverage focusing on its displacement across time. First, it builds two indices that quantify the degree to which its observed distribution deviates from a fully coherent expansion/recession pattern (i.e., inundation displacement). Second, it maps displacement with these indices over the last 36 years for the whole globe using remotely sensed data of surface water and evaluates their conjoint performance across gradients of coherence. Finally, it explores how inundation displacement relates to natural and anthropic factors. The ultimate goal is to set the methodological basis for studying displacement patterns and trends using long-term data of global scope.

## 2. Data and Methods

We based our work on high-resolution, remotely sensed data of surface water coverage, using spatially aggregated (single pixels within a grid cell) time series versus temporally aggregated (single dates across the whole study period) pixel distributions to quantify displacement. The monthly, 30-m resolution Global Surface Water data set (Pekel et al., 2016a) is powerful to analyze regional-level inundation processes, with observations

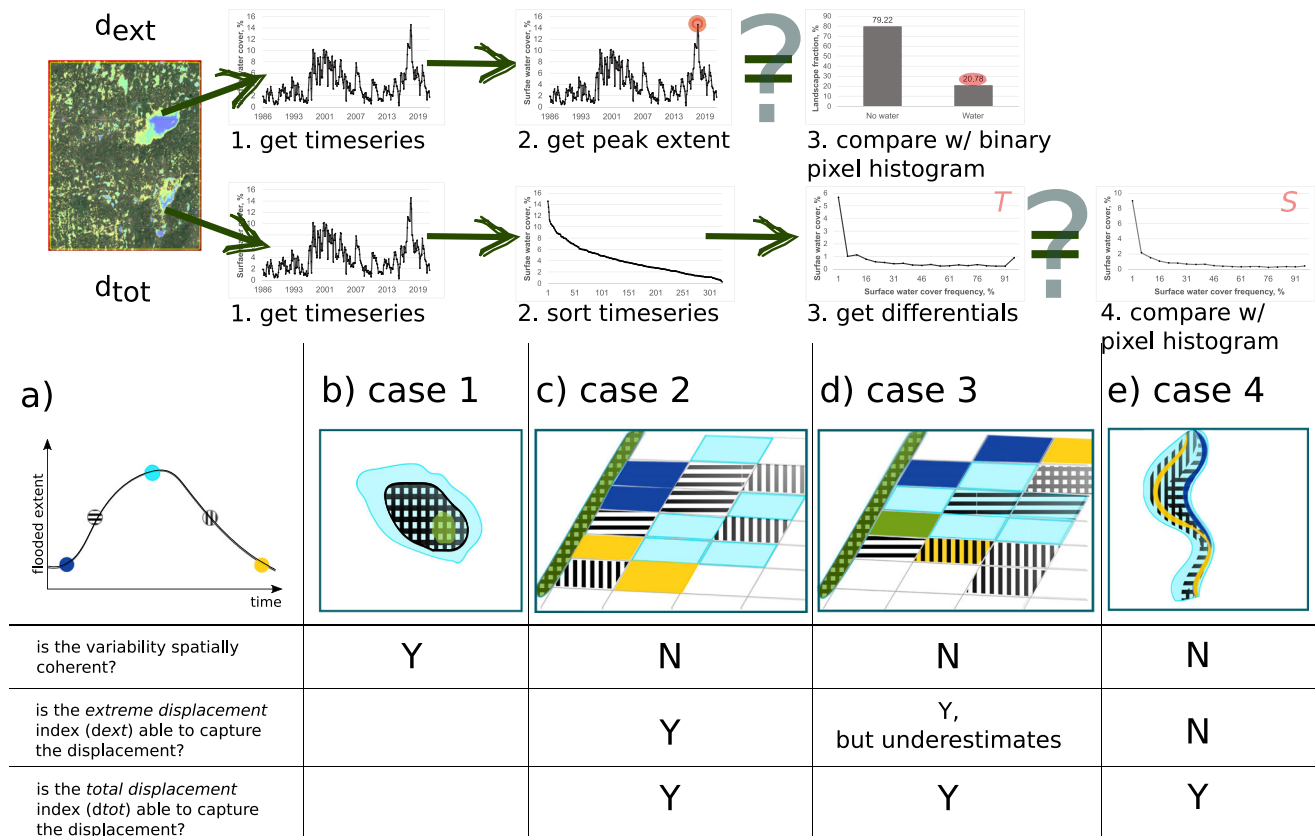


**Figure 1.** Top panel: Schematic representation of the calculation and comparison of two inundation frequency distributions based on the time series of surface water coverage for a given territory (temporal analysis, T) and the contribution of its individual pixels (spatial analysis, S). Bottom panel: Four alternative hypothetical configurations of surface water dynamics that follow identical temporal series of spatially-aggregated water coverage (a). Cases include: (b) coherent dynamic where the last water-covered areas are the first to dry, commonly observed in lakes; (c) incoherent flooding dynamic where each plot is flooded in a rotative way such that each one is covered by water at only one time-step, a situation that could take place in low-to-medium intensity irrigated regions; (d) incoherent flooding dynamic where plots are alternately and variably covered by water, a situation expected in high intensity irrigated regions; (e) incoherent flooding dynamic where the spatial pattern of the wetting and drying phase diverges, which can be expected in branched and meandering rivers and their surrounding floodplains as well as hydrologically connected wetlands. Coherence and the ability of the two indices ( $d_{ext}$  and  $d_{tot}$ ) to capture displacement are indicated (yes/no).

going back as far as 1985. Its most recent version (v1.4) extended the original version up to 2021, inclusive, and can be found in the Google Earth Engine catalog, the latter which allows the processing of such vast amounts of data.

A spatially coherent development of surface water cover should reflect a bucket-like geometry where, as the inundated area increases, already flooded places stay covered by water, and where one can observe the same distribution of water-covered and water-free areas for any given fraction of total water coverage in the region overtime, regardless of being in the expansion or retraction phase (Figure 1b). In such cases, when water coverage is aggregated for a given extent of the territory (e.g., catchment or grid cell) the overall inundated area (sum of all the individual pixels that were covered by water at any point in time) should match the maximum water cover extent (sum of all the pixels covered by water at the region's peak), and its recession should mirror its development exactly with the first drying areas being the last ones that got flooded. Taking this hypothetical situation as a null model, we measured two aspects through which departures from this pattern can emerge. Three alternative hypothetical situations are schematized in Figures 1c–1e.

First, we defined the extreme displacement ( $d_{ext}$ ) as the relative difference between the overall water coverage (O), which is the sum of all pixels that were covered by water at any point in time, and the maximum extent observed simultaneously at any particular month in the spatially-aggregated time series (Mx) (Equation 1).

$$d_{ext} = \frac{O - Mx}{Mx} \quad (1)$$

This index represents the fraction of area that was engaged in inundation patterns but not during its peak and is assumed to have been gained from the dry fraction of the landscape. It then provides valuable information about the wetting-drying dynamic of the region. For this reason, it should be more sensitive for analyzing individual events or dynamics in which different fractions of the landscape engage as surface water expands, more commonly found in irrigated landscapes (Figure 1c).

The  $d_{ext}$  index may underestimate displacement taking place at intermediate stages of water coverage or highly rotating patterns, such as those experienced in high-intensity irrigated landscapes where the inundation sequence of plots is erratic (Figure 1d). It could also fall short of capturing dynamics where the engaged areas may converge beyond a certain threshold of water coverage but not below it (i.e., yielding  $d_{ext} = 0$ ; Figure 1e), and where, still, the observed apportionment of flooding frequency among pixels differs greatly from a coherent pattern. In such cases, the exceeding area does not result just from the dry fraction of the landscape but also from what we would expect to be permanently water-covered areas, producing more temporary water bodies than those derived from a spatially aggregated surface water time series.

Given the potential underestimation of displacements by the first index presented above, we constructed a total displacement index ( $d_{tot}$ ) by comparing two different surface water frequency distributions. The first one (temporal distribution,  $T$ ) results from sorting the time series of monthly surface water extent in a decreasing array. Assuming a null model where the aggregated monthly flood extent accurately represents the water dynamics within the region, this rearrangement would show (a) the maximum inundated area (i.e., the first observation where all pixels that can be covered by water are so); (b) the hydrologic baseline or permanent water fraction (i.e., the lowest extent observed, which could also be zero); and (c) the inundation frequency distribution per fraction of area, which is obtained by calculating the difference between observations, starting from the maximum. For example, a region where the maximum observed event across 10 years (i.e., 120 monthly observations) covered 1% of the area and the next biggest event accounted for 0.9%, should show 0.1% of its area with an inundation frequency of 1/120 (0.83%). Then, under the null model,  $T$  reflects the relative contribution of areas with different individual inundation frequencies, which can be estimated independently by measuring the distribution of the actual inundation frequencies, as the percentage of observations with water at the pixel level ( $30 \times 30 \text{ m}^2$ ) ( $S$ ). The mismatch between  $T$  and  $S$  can be quantified as shown in Equation 2 (Figure 1, top panel):

$$d_{tot} = \frac{\sum_0^{100} T_n - S_n}{Mx} \quad \text{for } T_n > S_n \quad (2)$$

where  $T_n$  and  $S_n$  are the areas showing  $n\%$  of inundation frequency under the temporal and spatial distributions, respectively. We standardized the mismatches to the maximum surface water extent event ( $Mx$ ) of the region, and thus  $d_{tot}$  expresses the equivalent fraction of  $Mx$  that shifts because of changing water-covered area locations within and between flooding events.

The described phenomenon can be characterized across multiple spatial scales of analyses, comparing upper-level behavior's concordance with their lower-level components' dynamic (e.g., pixels in remotely sensed data). For this global scope study, we chose a large landscape scale as our focal level, arranging a  $1^\circ$  grid ( $\sim 111 \times 111 \text{ km}$  at the Equator). After excluding cells that included the ocean surface (12,500 resulting cells), we obtained the landscape-level surface water extent for each cell and month between 1985 and 2021 and further filtered out (a) time series with  $<70\%$  of data available across the cell, and (b) grid cells having  $<0.1\%$  of maximum surface water extent or  $<30$  observations, to reduce noise effects. Thus, we analyzed 10,047 cells over all continents except Antarctica. To illustrate the applications of the displacement indices, we investigated the impact of natural and human factors on inundated location changes overtime. Boosted regression trees were used to relate water displacement with topographical, climatological, hydrological, and agricultural variables (see Supporting Information S1 for more details). The processing of the surface water extent data set was done in Google Earth Engine, and posterior analyses were completed in an R environment (R Core Team, 2021).

### 3. Results and Discussion

#### 3.1. Inundation Displacement Characterization

Based on remote sensing data, we developed a novel way to study how water moves across the surface revealing that its displacement, at varying degrees, is a widespread phenomenon, not only relevant in riverbanks but also

important in shallow lakes and irrigated areas worldwide. Both displacement indices ( $d_{ext}$  and  $d_{tot}$ ) were able to capture patterns where inundated areas change location overtime. We discovered that close-to-fully coherent patterns (i.e., no displacement) existed in lotic systems including floodplain sections across the Kunene, Ob and Paraguay Rivers in Angola, Russia, and Paraguay, respectively ( $d_{ext}$  and  $d_{tot} < 0.2$ ), while in other regions displacement was so large that it exposed up to five times more area to inundation than expected from a coherent pattern, for example, in the floodplains of the Ucayali and Purús rivers in South America ( $d_{ext}$  and  $d_{tot} > 1$ ) known for their high sediment load and dynamic geomorphology. Inundation displacement could result from different expansion patterns associated with altering water sources (Tockner et al., 2000), or from hysteretic patterns (i.e., non-symmetrical expansion/recession trajectories) related to riverine geomorphology (Poole, 2010). Yet, this pattern was also extended to lentic systems, for instance those in the northern Undulating Pampas in Argentina composed of very shallow lakes under a delicate, water table-mediated flood-generating mechanism (Kuppel et al., 2015). This suggested the indices' capability for discriminating sites in which different inundation mechanisms may prevail (Van Dijk et al., 2013; Wu et al., 2023), and even for comparing their actual development overtime against their simulated behavior (Camporeale et al., 2005; Rudorff et al., 2014).

Different inundation patterns fostering displacement became evident after comparing the performance of both indices across 10,047, 1°-gridded landscapes (Figure 2). Low values of both  $d_{ext}$  and  $d_{tot}$  were indicative of coherent patterns where water expanded and receded following the same geometrical path, such as that in well-defined lake basins (Figures 2a and 2b). Increases in either index could be attributed to redistribution of surface water overtime or within individual events. Greater differences in favor of  $d_{tot}$  (Figures 2d–2f) suggested shifting patterns with a maximum event that covers all floodable areas, as a result of intense rainfall, snowmelt, or upstream runoff pulses (e.g., Figure 1e). Despite an almost perfect overlap of maximum and overall coverage, up to 40% of the peak extent alternated over time. In certain riverplains (e.g., in sections of the Ob' River, Figure 2d), this behavior had a marginal impact, accounting for less than 20% of water cover shifts. Elsewhere, higher  $d_{tot}$  values illustrated the evaporative dynamics of the Eyasi Lake and Aral Sea in Eastern Africa and Central Asia (Figures 2e and 2f). This type of displacement was more representative of the greatest water-covered landscapes (Figure 2 top-left panel, blue points). Finally, visual interpretation of cells with very high values of  $d_{ext}$  and  $d_{tot}$  suggested their sensitivity to both natural and human imprints on the distribution of flooded areas (Figures 2g–2i).

Inundation displacement indices complement common hydrological attributes, highlighting the contribution of this novel approach (Figure S2 in Supporting Information S1). Typical indicators of inundation variability include minimum, mean, and maximum extents, and coefficient of variation derived from spatially-aggregated time series (e.g., Papa et al., 2008, 2010; Pickens et al., 2020). Our quantitative assessment of surface water redistribution appeared to complement its temporal analysis (i.e., were poorly correlated) based upon the aggregation of higher resolution data, independently of their magnitude (i.e., for rarely inundated regions as well as for those completely covered by water), or how temporally variable they were (i.e., from very stable to highly erratic floods). A sensitivity analysis of the indices to different window sizes revealed that our metrics were robust, exhibiting only limited sensitivity to alterations (See Supporting Information S1 for more details). These minor impacts were primarily associated with variations in large-scale synchronicity of surface water dynamics and the potential influence of remote sensing noise effects. These findings are suggestive of the value of the indices as, for instance, ephemeral and shallow water bodies fluctuating in size and volume, but also in location—as the indices capture—tend to be key contributors to greenhouse gas emissions (Saunois et al., 2020; Walcker et al., 2021), and whose wetting/drying dynamics may have been underestimated with current aggregation approaches (Davidson et al., 2018).

### 3.2. Global Patterns of Inundation Displacement

Regional clusters of high inundation displacement became evident after mapping the two indices ( $d_{ext}$  and  $d_{tot}$ ) globally (Figure 3). The general similarity between both indices suggested that the dominant displacement component is the shift of water masses (e.g., Figure 1c), while erratic rotation (of river channels or irrigated plots, e.g., Figure 1d) has a secondary role and only in a subset of regions. The geographical distribution of inundation displacement showed river valleys in South America and Central Asia with the greatest degrees of displacement (captured by both indices, e.g., Figures 2g–2i), followed by mountainous rivers and irrigation-dense regions further captured by the total displacement index (e.g., Figures 1d and 1e). The highest displacement took place in the tropics and subtropics associated with riverbeds hosting water courses that reach flat humid plains after

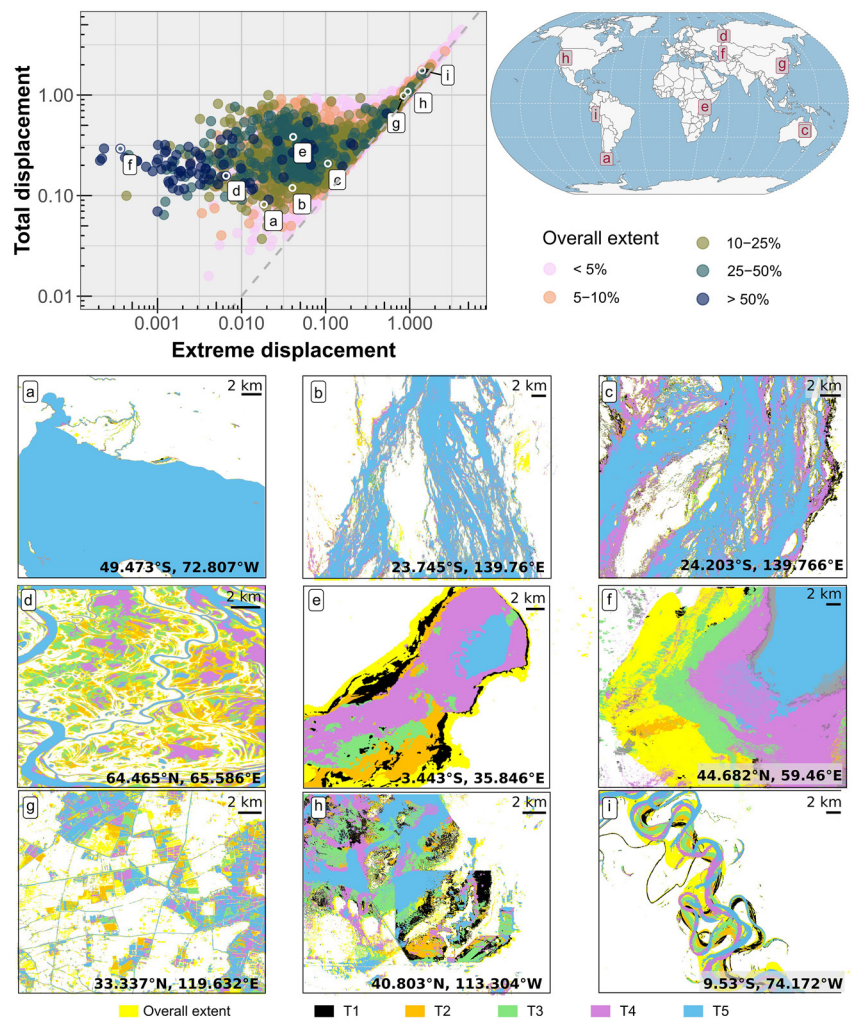


**Figure 2.** Values assumed for the two proposed inundation displacement indices (extreme displacement,  $d_{ext}$ , and total displacement,  $d_{tot}$ ) across 10,047  $1^\circ$  landscapes. Top-left panel: log-log scatter plot coloring cells according to their overall extent (i.e., the fraction of area that has been water-covered at least once in the last 36 years), with the gray dotted line reflecting the equality line between both indices. (a–i) Examples of the (mis)matches between the overall extent (yellow background) and the geographical contribution of fractions of the landscape in five moments (T1–T5). (a) Lake Viedma, Argentina; (b, c) Diamantina River, Australia; (d) Ob’ River, Russia; (e) Eyasi Lake, Tanzania; (f) Aral Sea, Kazakhstan; (g) Zhenjiang, China (triple cropping hotspot); (h) Salt Flats, United States (partially exploited); (i) Ucayali River, Perú.

leaving young mountain ranges with high sediment production (Chakrapani, 2005). Most of them were located at the base of Himalayas and Andes ranges where large alluvial fans tend to dominate the landscape, feeding sediments to braided and meandering rivers that transport them, likely driving massive flood displacements in these areas (Ayaz et al., 2018; Constantine & Dunne, 2008; Dhali et al., 2020; Horton & Decelles, 2001; Schwendel et al., 2015).

Besides tropical and subtropical hotspots of displacement fostered by large, and geomorphologically dynamic riverplains, the rest of the world appeared less affected by shifts in the maximum water-covered area, as captured by  $d_{ext}$ , with an average of 0.25 (i.e., 25% more engaged area than that covered by their highest individual event). Yet, some regions were characterized by patterns in which displacement at intermediate inundation stages was more prominent ( $d_{tot}$  averaged 0.45) (Figures 2d–2f). Examples of this behavior included the tundra shallow lakes region across the Canadian Shield and an irrigation-dense area along the northern edge of the Tibetan Plateau. Such cases were indicative of patterns where, outside high pulses that covered all floodable areas, there may have been shifts overtime between pulses, for instance through the alternation of single, double, and triple rice cropping in rice-intensive regions (Chen et al., 2012; Sakamoto et al., 2007; Tran et al., 2018). The regional

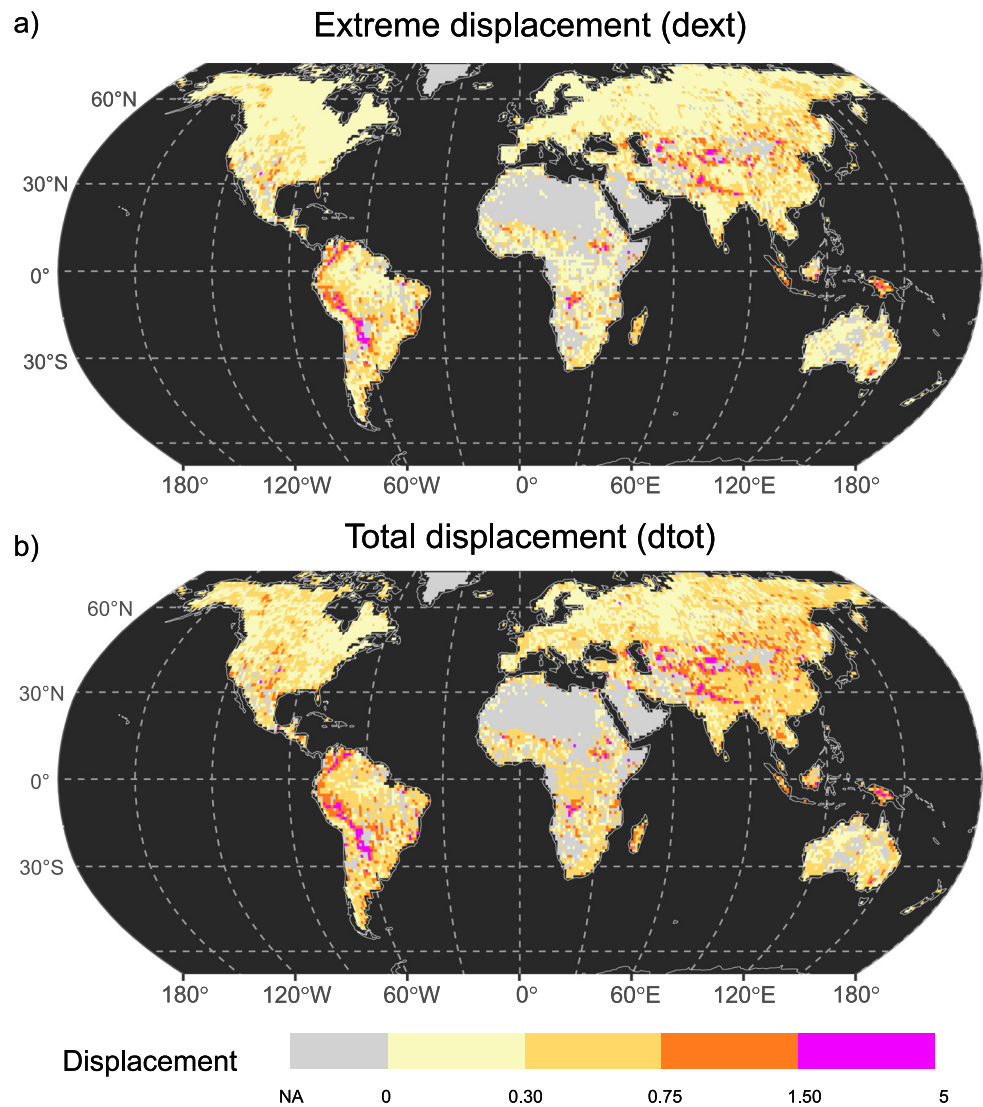


**Figure 3.** Global distribution of inundation displacement as described by two indices, (a) by obtaining the overall inundated area exceeding the maximum observed water-covered area at any particular month (extreme displacement,  $d_{ext}$ ), (b) by quantifying mismatches between the distribution of inundation frequency pixels and a null model given by the arrangement of landscape-aggregated time series of surface water extent (total displacement,  $d_{tot}$ ). An interactive online map is available at <https://torrezaffaroni.users.earthengine.app/view/walking-floods>.

imprint of flood irrigation for cropland production was detected through flooded patches shifting along tropical rivers in Central Asia as well as in other displacement hotspots found in rivers of other parts of central Asia (Yarkand and Aksu), southeastern Australia (Murray), and eastern China (Yellow and Yangtze). These areas match some of the most infrastructure-dense landscapes as evidenced in literature and through visual interpretation of high-definition images (Liu, 2022; Siebert et al., 2015; Zeng et al., 2016).

Remarkably, the lowest displacement ( $d_{ext}$  and  $d_{tot} < 0.3$ ) was characteristic of most of the boreal belt, especially across northern North America, Europe, and the vast majority of Russia. Local inundation dynamics were well captured at the landscape level with an approximate concentric expansion and retraction dynamic, possibly explained by the temperature-dominated (as opposed to precipitation-dominated) timing of floods (Kireeva et al., 2020; Papa et al., 2008; Torre Zaffaroni, Baldi, et al., 2023), the glacial processes that have shaped the topography of these landscapes in the past (i.e., a currently inactive geomorphological agent), and the role of permafrost in channeling water (Blöschl et al., 2020; Buttle et al., 2016; Rowland et al., 2023). It is crucial to note that these regions, due to the observed and potential effects of climate change on permafrost stocks

(Holgerson & Raymond, 2016; Schuur et al., 2015; Smith et al., 2022), may face increased rates of displacement and geomorphological alterations, putting at risk local and downstream communities and ecosystems (Lafrenière & Lamoureux, 2019).

### 3.3. Natural Versus Human Drivers of Inundation Displacement

Globally, natural drivers were on average more influential on inundation displacement than human drivers related to water management practices as shown by boosted regression trees (Figure S4 in Supporting Information S1, see Supporting Information S1 for more details). Across natural drivers, lake fraction, and local and regional indicators of ruggedness were the most important controls on inundation displacement. Extremely flat regions (regional terrain ruggedness index <80 m), despite pronounced local slopes, foster inundation displacement, aligning with the slower convergence effect observed in the absence of well-defined drainage systems (Figure S5 in Supporting Information S1) (Aragón et al., 2011; McGuire et al., 2005). The average distance between meanders, a quantitative indicator of river meandering, ranked fourth in influencing inundation displacement. This corroborated our observation that the indices can detect these highly dynamic landscapes, which provide numerous important ecosystem services worldwide (Angelini et al., 2013; Opperman et al., 2010; Walcker et al., 2021). Climate strongly affected displacement, with aridity (mean annual precipitation to potential evapotranspiration ratio <0.5) favoring it, perhaps due to higher spatial variability of precipitation events (Acworth et al., 2016; Griffin-Nolan et al., 2021; Tooth, 2000).

Across human drivers, the density of reservoir and irrigation infrastructure diminished and enhanced inundation displacement, respectively, with the latter being more influential even than paddy for rice and rainfed agriculture (Figure S5 in Supporting Information S1). Irrigation management's impact on this aspect of surface water emphasizes the need to consider its role in regional hydrology modeling. This can enhance the representation of multiple land and atmospheric processes, including greenhouse gas emissions and local climate variability (Houspanossian et al., 2018; Loarie et al., 2011; Saunio et al., 2020). Our findings were similar for  $d_{ext}$  (Figure S6 in Supporting Information S1), with lake fraction exerting greater influence than river meandering, and floodplain and irrigation coverage, possibly due to the lower capacity of this index in capturing such displacement patterns (Figures 1d and 1e).

Furthermore, the proposed indices may help in exploring how displacement changes in a given landscape as it is modified either gradually (e.g., due to increasing irrigation-allocated areas) or more abruptly (e.g., due to dam emplacements). As an example, we explored the landscape encompassing two water infrastructure projects in central China (Three Gorges Dam, built on the Yangtze River between 1994 and 2003, and the Shuibuya Dam built on the Qingjiang River between 2002 and 2008), revealing a sharp decrease of inundation displacement ( $d_{ext}$  from 1.42 to 0.43, Figure S7 in Supporting Information S1).

## 4. Conclusions

The distribution of water over a landscape and its variation through time is a critical but neglected aspect of hydrological analysis and its significance can be overlooked when examining aggregated water-covered areas over time. We tackled this gap by developing two indices, complementary to those typically employed to assess the temporal attributes of inundation, that capture the disparities between the actual spatiotemporal distribution of inundated areas in a landscape and a null model of spatially coherent dynamic in which water-covered areas expand and recede following symmetrical patterns in each event. Owing to this type of displacement, landscapes worldwide had 45% more area engaged in inundation patterns between 1985 and 2021 than what their single maximum levels may have indicated. The highest additions occurred in South American and Asian landscapes dominated by large meandering rivers transporting sediments from alluvial fans of the most tectonically active mountain ranges on Earth to their adjacent plains. Our results also showed that flat arid and tropical regions experienced the most significant displacement of water-covered areas due to natural and human influences, while boreal regions had the most spatially coherent dynamics, likely due to their glacially-shaped landscapes governed by permafrost.

The characterization of inundation displacement and its uniform application worldwide with the proposed indices have significant implications for understanding the influences of surface water on local and global climate as well as for evaluating the distant effects of land use change (e.g., deforestation irrigation and drainage infrastructure)



on hydrological regimes. Our indices demonstrated their ability to not only detect well-known, highly-dynamic inundation patterns across several floodplains, but also to further describe and quantify their effects on surface water dynamics worldwide evaluated through remote sensing. Through their adoption, we hope to stimulate further research on this aspect of the water cycle to a more comprehensive understanding of the complex dynamics of water in various landscapes.

### Conflict of Interest

The authors declare no conflicts of interest relevant to this study.

### Data Availability Statement

Global flooded extent was derived from JRC's Global Surface Water data set v1.4 (Pekel et al., 2016b) available in the Google Earth Engine Data Catalog. Anthromes were downloaded from Ellis and Klein Goldewijk (2019). River segment characterization was extracted from Frasson et al. (2019) based on Global River Width from Landsat. Global Lakes and Wetlands Database Level 3 (GLWD-3) was downloaded from Lehner and Döll (2004). The aridity index was calculated based on TerraClimate long-term averages of annual precipitation-to-potential evapotranspiration ratios (Abatzoglou et al., 2018), while terrain attributes were calculated based on Global Multi-resolution Terrain Data set (USGS), both available in the Google Earth Engine Data Catalog. The codes for characterizing displacement in Google Earth Engine and analyzing it in R, along with the database, with all variables aggregated to the 1° grid, can be found at Torre Zaffaroni, Houspanossian, et al. (2023).

### Acknowledgments

This work was supported by CONICET (PIP 11220200100363CO, PIBBA 28720210100697CO). We thank the editor and anonymous reviewers for their valuable comments which have improved our work. We extend our thanks to Germán Baldi, Tomas Milani, Marcos Niborski, María Poca, and Luciana Staiano for their constructive inputs at different stages.

### References

- Abatzoglou, J. T., Dobrowski, S. Z., Parks, S. A., & Hegewisch, K. C. (2018). TerraClimate: Monthly climate and climatic water balance for global terrestrial surfaces. University of Idaho [Dataset]. <https://doi.org/10.1038/sdata.2017.191>
- Acworth, R. I., Rau, G. C., Cuthbert, M. O., Jensen, E., & Leggett, K. (2016). Long-term spatio-temporal precipitation variability in arid-zone Australia and implications for groundwater recharge. *Hydrogeology Journal*, 24(4), 905–921. <https://doi.org/10.1007/s10040-015-1358-7>
- Angelini, R., de Morais, R. J., Catella, A. C., Resende, E. K., & Libralato, S. (2013). Aquatic food webs of the oxbow lakes in the Pantanal: A new site for fisheries guaranteed by alternated control? *Ecological Modelling*, 253, 82–96. <https://doi.org/10.1016/j.ecolmodel.2013.01.001>
- Aragón, R., Jobbágy, E. G., & Viglizzo, E. F. (2011). Surface and groundwater dynamics in the sedimentary plains of the Western Pampas (Argentina). *Ecohydrology*, 4(3), 433–447. <https://doi.org/10.1002/eco.149>
- Arias, P., Bellouin, N., Coppola, E., Jones, R., Krinner, G., Marotzke, J., et al. (2021). *Technical summary* (Tech. Rep.). The Intergovernmental Panel on Climate Change (IPCC).
- Ayaz, S., Biswas, M., & Dhali, M. K. (2018). Morphotectonic analysis of alluvial fan dynamics: Comparative study in spatio-temporal scale of Himalayan foothill, India. *Arabian Journal of Geosciences*, 11(2), 1–16. <https://doi.org/10.1007/S12517-017-3308-2/TABLES/5>
- Blöschl, G., Kiss, A., Viglione, A., Barriendos, M., Böhm, O., Brázdil, R., et al. (2020). Current European flood-rich period exceptional compared with past 500 years. *Nature*, 583(7817), 560–566. <https://doi.org/10.1038/s41586-020-2478-3>
- Brunsell, N. A. (2010). A multiscale information theory approach to assess spatial-temporal variability of daily precipitation. *Journal of Hydrology*, 385(1–4), 165–172. <https://doi.org/10.1016/j.jhydrol.2010.02.016>
- Buttle, J. M., Allen, D. M., Caissie, D., Davison, B., Hayashi, M., Peters, D. L., et al. (2016). Flood processes in Canada: Regional and special aspects. *Canadian Water Resources Journal/Revue Canadienne des Ressources Hydriques*, 41(1–2), 7–30. <https://doi.org/10.1080/07011784.2015.1131629>
- Camporeale, C., Perona, P., Porporato, A., & Ridolfi, L. (2005). On the long-term behavior of meandering rivers. *Water Resources Research*, 41(12), W12403. <https://doi.org/10.1029/2005WR004109>
- Chakrapani, G. J. (2005). Factors controlling variations in river sediment loads. *Current Science*, 88(4), 569–575.
- Chen, C. F., Son, N. T., & Chang, L. Y. (2012). Monitoring of rice cropping intensity in the upper Mekong Delta, Vietnam using time-series MODIS data. *Advances in Space Research*, 49(2), 292–301. <https://doi.org/10.1016/j.asr.2011.09.011>
- Constantine, J. A., & Dunne, T. (2008). Meander cutoff and the controls on the production of oxbow lakes. *Geology*, 36(1), 23–26. <https://doi.org/10.1130/G24130A.1>
- Davison, N. C., Fluet-Chouinard, E., & Finlayson, C. M. (2018). Global extent and distribution of wetlands: Trends and issues. *Marine and Freshwater Research*, 69(4), 620–627. <https://doi.org/10.1071/MF17019>
- Dhali, M. K., Ayaz, S., Sahana, M., & Guha, S. (2020). Response of sediment flux, bridge scouring on river bed morphology and geomorphic resilience in middle-lower part of river Chel, Eastern Himalayan foothills zone, India. *Ecological Engineering*, 142, 105632. <https://doi.org/10.1016/j.ecoleng.2019.105632>
- Dong, J., Xiao, X., Kou, W., Qin, Y., Zhang, G., Li, L., et al. (2015). Tracking the dynamics of paddy rice planting area in 1986–2010 through time series Landsat images and phenology-based algorithms. *Remote Sensing of Environment*, 160, 99–113. <https://doi.org/10.1016/j.rse.2015.01.004>
- Ellis, E., & Klein Goldewijk, K. (2019). Anthromes 12k full dataset [Dataset]. <https://doi.org/10.7910/DVN/G0QDNQ>
- Finotello, A., D'Alpaos, A., Bogoni, M., Ghinassi, M., & Lanzoni, S. (2020). Remotely-sensed planform morphologies reveal fluvial and tidal nature of meandering channels. *Scientific Reports*, 10(1), 1–13. <https://doi.org/10.1038/s41598-019-56992-w>
- Frasson, R. P. D. M., Pavelsky, T. M., Fonstad, M. A., Durand, M. T., Allen, G. H., Schumann, G., et al. (2019). Global database of river width, slope, catchment area, meander wavelength, sinuosity, and discharge [Dataset]. Zenodo. <https://doi.org/10.5281/zenodo.2582500>
- Gardner, J. R., Yang, X., Topp, S. N., Ross, M. R., Altenau, E. H., & Pavelsky, T. M. (2021). The color of rivers. *Geophysical Research Letters*, 48(1), e2020GL088946. <https://doi.org/10.1029/2020GL088946>

- Gorelick, N., Hancher, M., Dixon, M., Ilyushchenko, S., Thau, D., & Moore, R. (2017). Google Earth Engine: Planetary-scale geospatial analysis for everyone. *Remote Sensing of Environment*, 202, 18–27. <https://doi.org/10.1016/j.rse.2017.06.031>
- Griffin-Nolan, R. J., Slette, I. J., & Knapp, A. K. (2021). Deconstructing precipitation variability: Rainfall event size and timing uniquely alter ecosystem dynamics. *Journal of Ecology*, 109(9), 3356–3369. <https://doi.org/10.1111/1365-2745.13724>
- Holgerson, M. A., & Raymond, P. A. (2016). Large contribution to inland water CO<sub>2</sub> and CH<sub>4</sub> emissions from very small ponds. *Nature Geoscience*, 9(3), 222–226. <https://doi.org/10.1038/ngeo2654>
- Horton, B. K., & Decelles, P. G. (2001). Modern and ancient fluvial megafans in the foreland basin system of the Central Andes, Southern Bolivia: Implications for drainage network evolution if foldthrust belts. *Basin Research*, 13(1), 43–63. <https://doi.org/10.1046/j.1365-2117.2001.00137.x>
- Houspanossian, J., Kuppel, S., Nosetto, M. D., Di Bella, C. M., Oricchio, P., Barrucand, M., et al. (2018). Long-lasting floods buffer the thermal regime of the Pampas. *Theoretical and Applied Climatology*, 131(1–2), 111–120. <https://doi.org/10.1007/s00704-016-1959-7>
- Junk, W., Bayley, P., & Sparks, R. (1989). The flood pulse concept in river-floodplain systems. In *Canadian Special Publication of Fisheries and Aquatic Sciences* (Vol. 106, pp. 110–127).
- Kireeva, M. B., Rets, E. P., Frolova, N. L., Samsonov, T. E., Povalishnikova, E. S., Entin, A. L., et al. (2020). Occasional floods on the rivers of Russian plain in the 20th–21st centuries. *Geography, Environment, Sustainability*, 13(2), 84–95. <https://doi.org/10.24057/2071-9388-2020-29>
- Kundzewicz, Z. W. (2008). Climate change impacts on the hydrological cycle. *Ecology and Hydrobiology*, 8(2–4), 195–203. <https://doi.org/10.2478/v10104-009-0015-y>
- Kuppel, S., Houspanossian, J., Nosetto, M. D., & Jobbágy, E. G. (2015). What does it take to flood the Pampas?: Lessons from a decade of strong hydrological fluctuations. *Water Resources Research*, 51(4), 2937–2950. <https://doi.org/10.1002/2015WR016966>
- Lafrènière, M. J., & Lamoureux, S. F. (2019). *Effects of changing permafrost conditions on hydrological processes and fluvial fluxes* (Vol. 191). Elsevier. <https://doi.org/10.1016/j.earscirev.2019.02.018>
- Langhorst, T., & Pavelsky, T. (2023). Global observations of riverbank erosion and accretion from Landsat imagery. *Journal of Geophysical Research: Earth Surface*, 128(2), e2022JF006774. <https://doi.org/10.1029/2022JF006774>
- Lehner, B., & Döll, P. (2004). Global lakes and wetlands database: Lakes and wetlands grid (level 3) [Dataset]. World Wildlife Fund. Retrieved from <https://www.worldwildlife.org/publications/global-lakes-and-wetlands-database-lakes-and-wetlands-grid-level-3>
- Lin, P., Pan, M., Allen, G. H., de Frasson, R. P., Zeng, Z., Yamazaki, D., & Wood, E. F. (2020). Global estimates of reach-level bankfull river width leveraging big data geospatial analysis. *Geophysical Research Letters*, 47(7), e2019GL086405. <https://doi.org/10.1029/2019GL086405>
- Liu, G. (2022). Understanding cotton cultivation dynamics in Aksu Oases (NW China) by reconstructing change trajectories using multi-temporal Landsat and Sentinel-2 data. *Geocarto International*, 37(15), 4406–4424. <https://doi.org/10.1080/10106049.2021.1886337>
- Loarie, S. R., Lobell, D. B., Asner, G. P., & Field, C. B. (2011). Land-cover and surface water change drive large albedo increases in South America\*. *Earth Interactions*, 15(7), 1–16. <https://doi.org/10.1175/2010EI342.1>
- McGuire, K. J., McDonnell, J. J., Weiler, M., Kendall, C., McGlynn, B. L., Welker, J. M., & Seibert, J. (2005). The role of topography on catchment-scale water residence time. *Water Resources Research*, 41(5), 1–14. <https://doi.org/10.1029/2004WR003657>
- Najibi, N., & Devineni, N. (2018). Recent trends in the frequency and duration of global floods. *Earth System Dynamics*, 9(2), 757–783. <https://doi.org/10.5194/esd-9-757-2018>
- Olthof, I., & Rainville, T. (2022). Dynamic surface water maps of Canada from 1984 to 2019 Landsat satellite imagery. *Remote Sensing of Environment*, 279, 113121. <https://doi.org/10.1016/j.rse.2022.113121>
- Opperman, J. J., Luster, R., McKenney, B. A., Roberts, M., & Meadows, A. W. (2010). Ecologically functional floodplains: Connectivity, flow regime, and scale. *Journal of the American Water Resources Association*, 46(2), 211–226. <https://doi.org/10.1111/j.1752-1688.2010.00426.x>
- Papa, F., Güntner, A., Frappart, F., Prigent, C., & Rossow, W. B. (2008). Variations of surface water extent and water storage in large river basins: A comparison of different global data sources. *Geophysical Research Letters*, 35(11), L11401. <https://doi.org/10.1029/2008GL033857>
- Papa, F., Prigent, C., Aires, F., Jimenez, C., Rossow, W. B., & Matthews, E. (2010). Interannual variability of surface water extent at the global scale, 1993–2004. *Journal of Geophysical Research*, 115(D12), D12111. <https://doi.org/10.1029/2009JD012674>
- Pekel, J.-F., Cottam, A., Gorelick, N., & Belward, A. S. (2016a). High-resolution mapping of global surface water and its long-term changes. *Nature*, 540(7633), 418–422. <https://doi.org/10.1038/nature20584>
- Pekel, J.-F., Cottam, A., Gorelick, N., & Belward, A. S. (2016b). High-resolution mapping of global surface water and its long-term changes [Dataset]. Nature Publishing Group. <https://doi.org/10.1038/nature20584>
- Pi, X., Luo, Q., Feng, L., Xu, Y., Tang, J., Liang, X., et al. (2022). Mapping global lake dynamics reveals the emerging roles of small lakes. *Nature Communications*, 13(1), 1–12. <https://doi.org/10.1038/s41467-022-33239-3>
- Pickens, A. H., Hansen, M. C., Hancher, M., Stehman, S. V., Tyukavina, A., Potapov, P., et al. (2020). Mapping and sampling to characterize global inland water dynamics from 1999 to 2018 with full Landsat time-series. *Remote Sensing of Environment*, 243(December 2019), 111792. <https://doi.org/10.1016/j.rse.2020.111792>
- Poole, G. C. (2010). Stream hydrogeomorphology as a physical science basis for advances in stream ecology. *Journal of the North American Benthological Society*, 29(1), 12–25. <https://doi.org/10.1899/08-070.1>
- R Core Team. (2021). R: A language and environment for statistical computing [Computer software manual]. Retrieved from <https://www.R-project.org/>
- Richardson, J., Sangree, J., & Sneider, R. (1987). Meandering stream reservoirs. *Journal of Petroleum Technology*, 39(12), 1501–1502. <https://doi.org/10.2118/15781-PA>
- Rowland, J. C., Schwenk, J. P., Shelef, E., Muss, J., Ahrens, D., Stauffer, S., et al. (2023). Scale-dependent influence of permafrost on riverbank erosion rates. *Journal of Geophysical Research: Earth Surface*, 128(7), e2023JF007101. <https://doi.org/10.1029/2023JF007101>
- Rudorff, C. M., Melack, J. M., & Bates, P. D. (2014). Flooding dynamics on the lower Amazon floodplain: 1. Hydraulic controls on water elevation, inundation extent, and river-floodplain discharge. *Water Resources Research*, 50(1), 619–634. <https://doi.org/10.1002/2013WR014091>
- Sakamoto, T., Van Nguyen, N., Kotera, A., Ohno, H., Ishitsuka, N., & Yokozawa, M. (2007). Detecting temporal changes in the extent of annual flooding within the Cambodia and the Vietnamese Mekong Delta from MODIS time-series imagery. *Remote Sensing of Environment*, 109(3), 295–313. <https://doi.org/10.1016/j.rse.2007.01.011>
- Saunio, M., Stavert, A. R., Poulter, B., Bousquet, P., Canadell, J. G., Jackson, R. B., et al. (2020). The global methane budget 2000–2017. *Earth System Science Data*, 12(3), 1561–1623. <https://doi.org/10.5194/essd-12-1561-2020>
- Schuur, E. A. G., McGuire, A. D., Schädel, C., Grosse, G., Harden, J. W., Hayes, D. J., et al. (2015). Climate change and the permafrost carbon feedback. *Nature*, 520(7546), 171–179. <https://doi.org/10.1038/nature14338>
- Schwendel, A. C., Nicholas, A. P., Aalto, R. E., Sambrook Smith, G. H., & Buckley, S. (2015). Interaction between meander dynamics and floodplain heterogeneity in a large tropical sand-bed river: The Rio Beni, Bolivian Amazon. *Earth Surface Processes and Landforms*, 40(15), 2026–2040. <https://doi.org/10.1002/esp.3777>

- Siebert, S., Kummu, M., Porkka, M., Döll, P., Ramankutty, N., & Scanlon, B. R. (2015). A global data set of the extent of irrigated land from 1900 to 2005. *Hydrology and Earth System Sciences*, *19*(3), 1521–1545. <https://doi.org/10.5194/hess-19-1521-2015>
- Sivapalan, M., Thompson, S. E., Harman, C. J., Basu, N. B., & Kumar, P. (2011). Water cycle dynamics in a changing environment: Improving predictability through synthesis. *Water Resources Research*, *47*(10). <https://doi.org/10.1029/2011WR011377>
- Smith, S. L., O'Neill, H. B., Isaksen, K., Noetzi, J., & Romanovsky, V. E. (2022). The changing thermal state of permafrost. *Nature Reviews Earth & Environment*, *3*(1), 10–23. <https://doi.org/10.1038/s43017-021-00240-1>
- Tena, A., Piégay, H., Seignemartin, G., Barra, A., Berger, J. F., Mourier, B., & Winiarski, T. (2020). Cumulative effects of channel correction and regulation on floodplain terrestrialisation patterns and connectivity. *Geomorphology*, *354*, 107034. <https://doi.org/10.1016/j.geomorph.2020.107034>
- Tockner, K., Malard, F., & Ward, J. V. (2000). An extension of the flood pulse concept. *Hydrological Processes*, *14*(16–17), 2861–2883. [https://doi.org/10.1002/1099-1085\(200011/12\)14:16/17\(2861::AID-HYP124\)3.0.CO;2-F](https://doi.org/10.1002/1099-1085(200011/12)14:16/17(2861::AID-HYP124)3.0.CO;2-F)
- Tockner, K., & Stanford, J. A. (2002). Riverine flood plains: Present state and future trends. *Environmental Conservation*, *29*(3), 308–330. <https://doi.org/10.1017/S037689290200022X>
- Tooth, S. (2000). Process, form and change in dryland rivers: A review of recent research. *Earth-Science Reviews*, *51*(1–4), 67–107. [https://doi.org/10.1016/S0012-8252\(00\)00014-3](https://doi.org/10.1016/S0012-8252(00)00014-3)
- Torre Zaffaroni, P., Baldi, G., Texeira, M., Di Bella, C. M., & Jobbágy, E. G. (2023). The timing of global floods and its association with climate and topography. *Water Resources Research*, *59*(7), e2022WR032968. <https://doi.org/10.1029/2022wr032968>
- Torre Zaffaroni, P., Houspanossian, J., Di Bella, C. M., & Jobbágy, E. G. (2023). Space-time inconsistencies in the dynamics of water coverage: Tracking walking floods [Software]. Zenodo. <https://doi.org/10.5281/zenodo.8083689>
- Tran, D. D., van Halsema, G., Hellegers, P. J., Ludwig, F., & Wyatt, A. (2018). Questioning triple rice intensification on the Vietnamese Mekong delta floodplains: An environmental and economic analysis of current land-use trends and alternatives. *Journal of Environmental Management*, *217*, 429–441. <https://doi.org/10.1016/j.jenvman.2018.03.116>
- Twine, T. E., Kucharik, C. J., & Foley, J. A. (2004). Effects of land cover change on the energy and water balance of the Mississippi River Basin. *Journal of Hydrometeorology*, *5*(4), 640–655. [https://doi.org/10.1175/1525-7541\(2004\)005\(0640:EOLCCO\)2.0.CO;2](https://doi.org/10.1175/1525-7541(2004)005(0640:EOLCCO)2.0.CO;2)
- Van Dijk, W. M., Van de Lageweg, W. I., & Kleinmans, M. G. (2013). Formation of a cohesive floodplain in a dynamic experimental meandering river. *Earth Surface Processes and Landforms*, *38*(13), 1550–1565. <https://doi.org/10.1002/ESP.3400>
- Vörösmarty, C. J., McIntyre, P. B., Gessner, M. O., Dudgeon, D., Prusevich, A., Green, P., et al. (2010). Global threats to human water security and river biodiversity. *Nature*, *467*(7315), 555–561. <https://doi.org/10.1038/nature09440>
- Walcker, R., Corenblit, D., Julien, F., Martinez, J.-M., & Steiger, J. (2021). Contribution of meandering rivers to natural carbon fluxes: Evidence from the Ucayali River, Peruvian Amazonia. *Science of the Total Environment*, *776*, 146056. <https://doi.org/10.1016/j.scitotenv.2021.146056>
- Wantzen, K. M., Junk, W. J., & Rothhaupt, K.-O. (2008). An extension of the floodpulse concept (FPC) for lakes. In *Ecological effects of water-level fluctuations in lakes* (pp. 151–170). Springer Netherlands. [https://doi.org/10.1007/978-1-4020-9192-6\\_15](https://doi.org/10.1007/978-1-4020-9192-6_15)
- Ward, J. V., & Stanford, J. A. (1995). Ecological connectivity in alluvial river ecosystems and its disruption by flow regulation. *Regulated Rivers: Research & Management*, *11*(1), 105–119. <https://doi.org/10.1002/rrr.3450110109>
- Watts, J. D., Kimball, J. S., Bartsch, A., & McDonald, K. C. (2014). Surface water inundation in the boreal-Arctic: Potential impacts on regional methane emissions. *Environmental Research Letters*, *9*(7), 075001. <https://doi.org/10.1088/1748-9326/9/7/075001>
- Wren, D. G., Davidson, G. R., Walker, W. G., & Galicki, S. J. (2008). The evolution of an oxbow lake in the Mississippi alluvial floodplain. *Journal of Soil and Water Conservation*, *63*(3), 129–135. <https://doi.org/10.2489/jswc.63.3.129>
- Wu, J., Zhang, Q., Li, Y., Xu, C. Y., & Ye, X. (2023). Spatial-temporal variations of stage-area hysteretic relationships in large heterogeneous lake–floodplain systems. *Journal of Hydrology*, *620*, 129507. <https://doi.org/10.1016/j.jhydrol.2023.129507>
- Zeng, Z.-H., Lu, Z.-Y., Jiang, Y., Zhang, K., Yang, Y.-D., & Zhao, P.-Y. (2016). Legume-cereal crop rotation systems in China. In *Crop rotations: Farming practices, monitoring and environmental benefits* (pp. 51–70). Nova Science Publishers.

## References From the Supporting Information

- Allen, G. H., & Pavelsky, T. (2018). Global extent of rivers and streams. *Science*, *361*(6402), 585–588. <https://doi.org/10.1126/science.aat063>
- Elith, J., Leathwick, J. R., & Hastie, T. (2008). *A working guide to boosted regression trees* (Vol. 77, No. (4)). John Wiley & Sons, Ltd. <https://doi.org/10.1111/j.1365-2656.2008.01390.x>
- Radinger, J., Alcaraz-Hernández, J. D., & García-Berthou, E. (2018). Environmental and spatial correlates of hydrologic alteration in a large Mediterranean river catchment. *Science of the Total Environment*, *639*, 1138–1147. <https://doi.org/10.1016/J.SCITOTENV.2018.05.227>
- Riley, S., DeGloria, S., & Elliot, R. (1999). A terrain ruggedness that quantifies topographic heterogeneity. *Intermountain Journal of Sciences*, *5*(1–4), 23–27.